Electronic Supplementary Material (ESI) for Dalton Transactions.

Supporting Information

Mono-/Bimetallic Water-Stable Lanthanide Coordination Polymers as Luminescent Probe for Detecting Cations, Anions and Organic Solvent Molecules

Huarui Wang[a,b], *Jianhua Qin*[a,b], *Chao Huang*[a], *Yanbing Han*[a], *Wenjuan Xu*[a], *Hongwei Hou*[a,]*

[a] College of Chemistry and Molecular Engineering,
Zhengzhou University, Henan, 450001, P. R. China
[b] College of Chemistry and Chemical Engineering
and Henan Key Laboratory of Function Oriented Porous Materials,
Luoyang Normal University, Henan, 471934, P. R. China

E-mail: houhongw@zzu.edu.cn; Fax: (86)371-67761744

Contents

1. **PXRD Patterns and Solid-State Luminescent Spectra Studies of 1-11 ……………….. S2**
2. **Thermal and Water Stability……………………………………………………………..S7**
3. **Sensing of Metal Cations……………………………………………………………………S9**
4. **Sensing of Anions ………………………………………………………………………… S12**
5. **Sensing of Organic Solvent Molecules …………………………………………………...S14**

6. Tables……………………………………………………………………………………S17

1. PXRD Patterns and Solid-State Luminescent Spectra Studies of 1-11

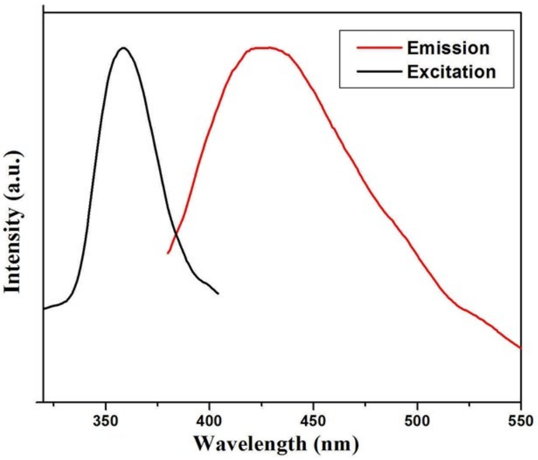

(a)

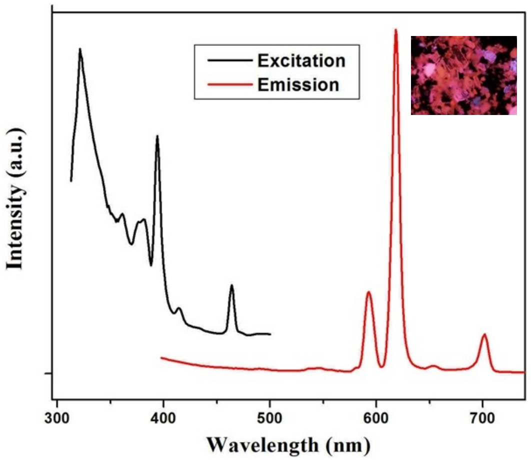

(b)

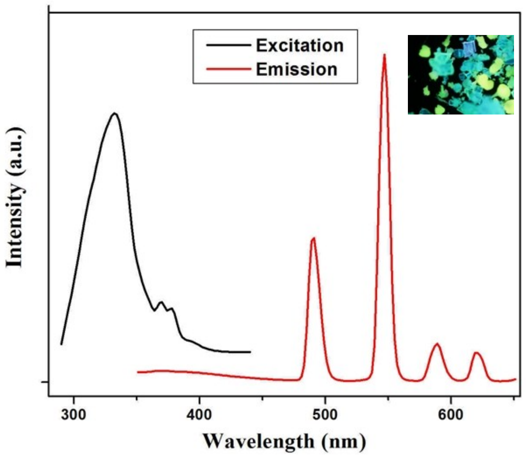

(c)

Figure S1. The emission spectra of the solid-state complexes: (a) H_4L ligand; (b) **1**; (c) **2**; (inset) the image of corresponding compound under the irradiation of 365 nm UV light.

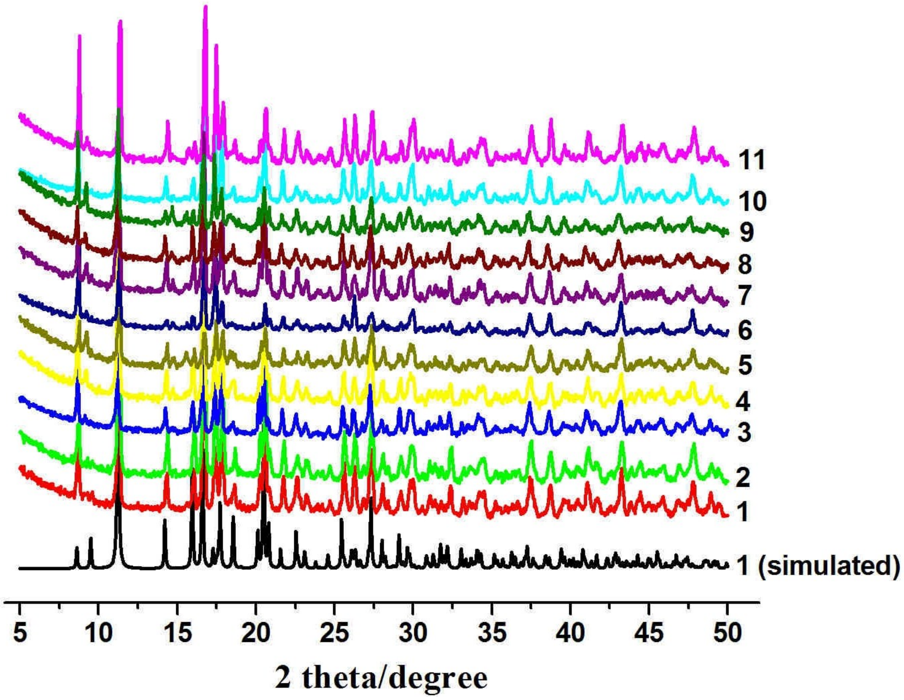

Figure S2. Powder X-ray diffraction patterns of CPs **1-11**.

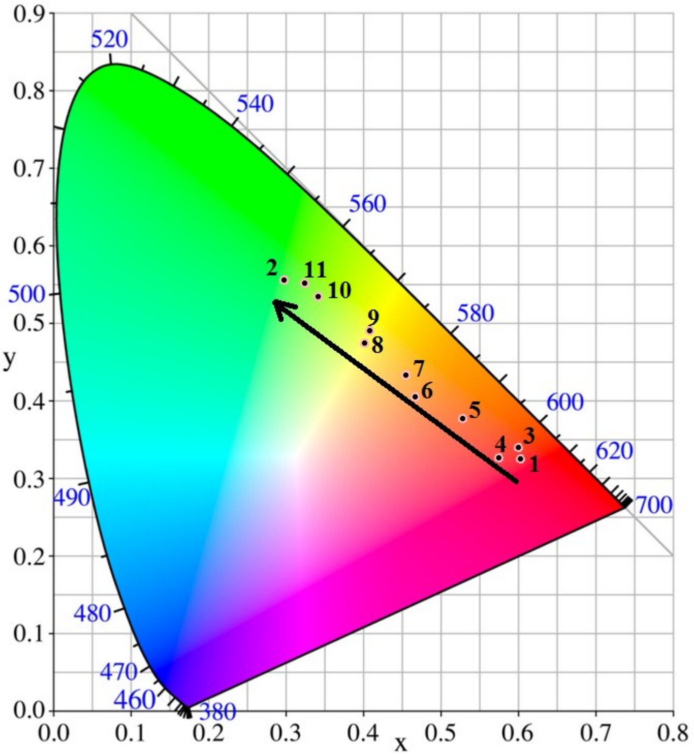

Figure S3. CIE chromaticity coordinates for **1**, **2**, and $\{[Eu_xTb_{1-x}(HL)(H_2O)_3]\cdot H_2O\}_n$ **3–11** when excited at 331 nm.

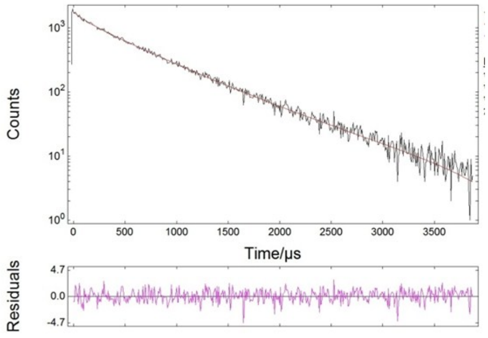

CP **1**

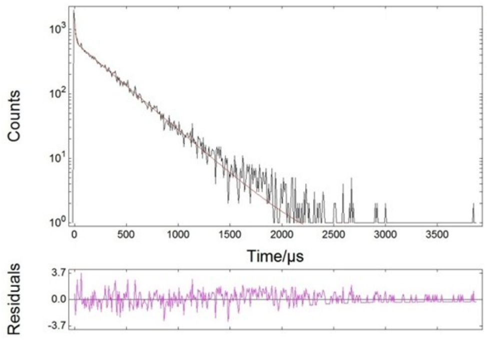

CP **2**

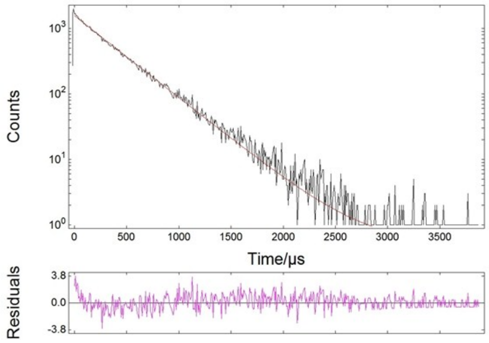

CP **3**

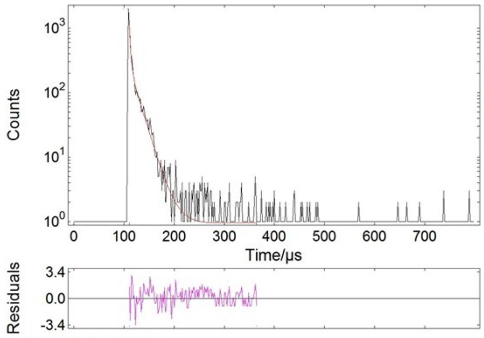

CP **3**

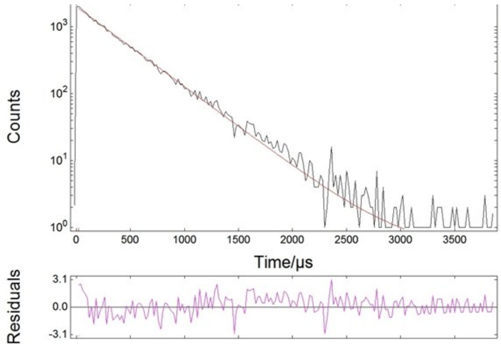

CP **4**

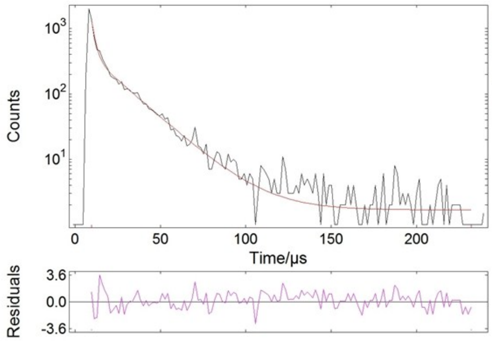

CP **4**

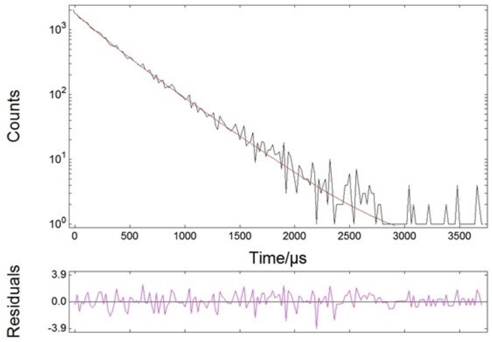

CP **5**

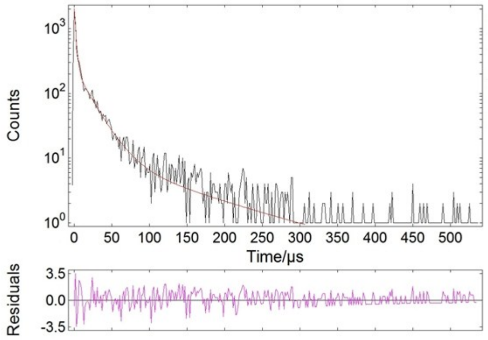

CP **5**

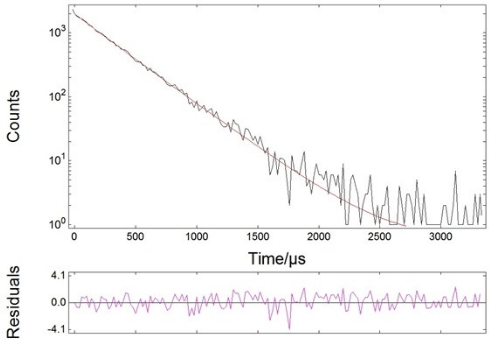

CP **6**

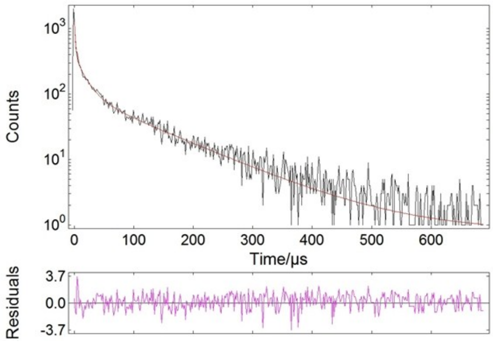

CP **6**

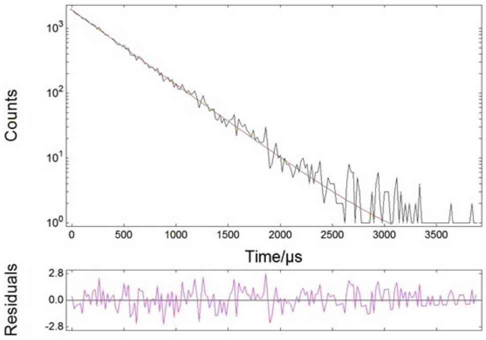

CP **7**

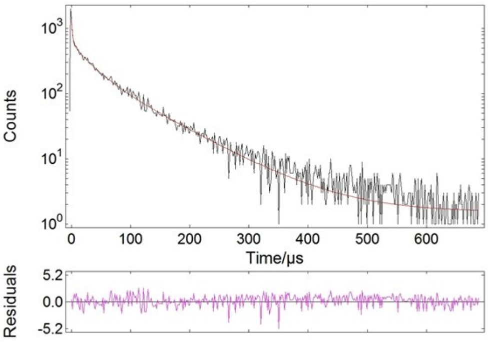

CP **7**

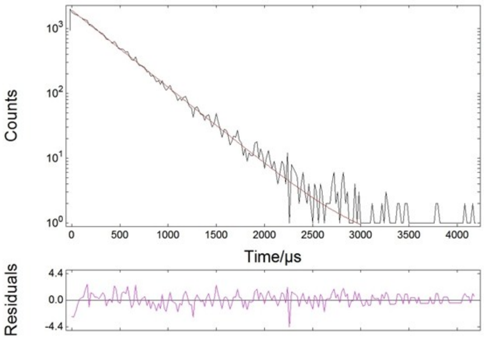

CP **8**

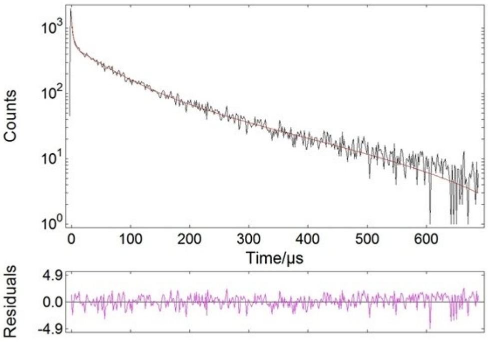

CP **8**

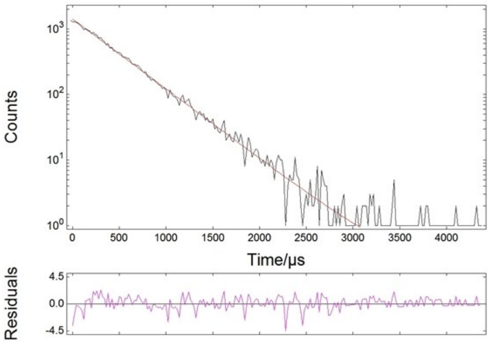

CP **9**

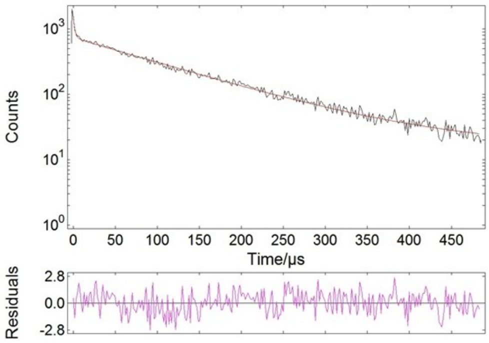

CP **9**

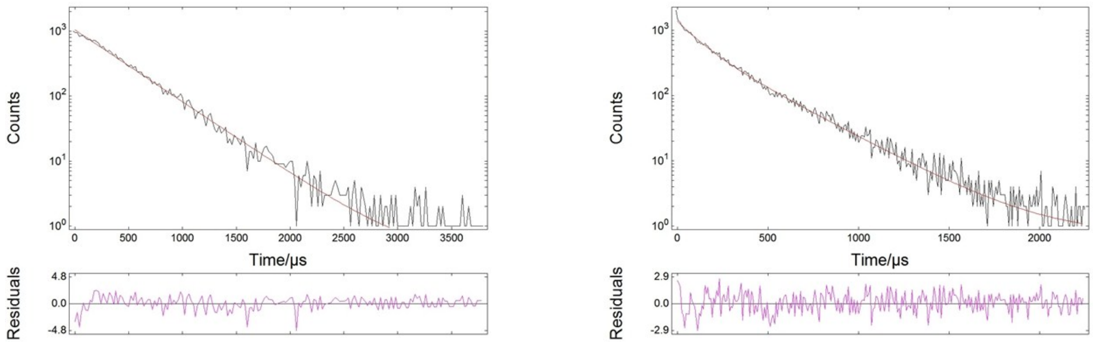

CP **10** CP **10**

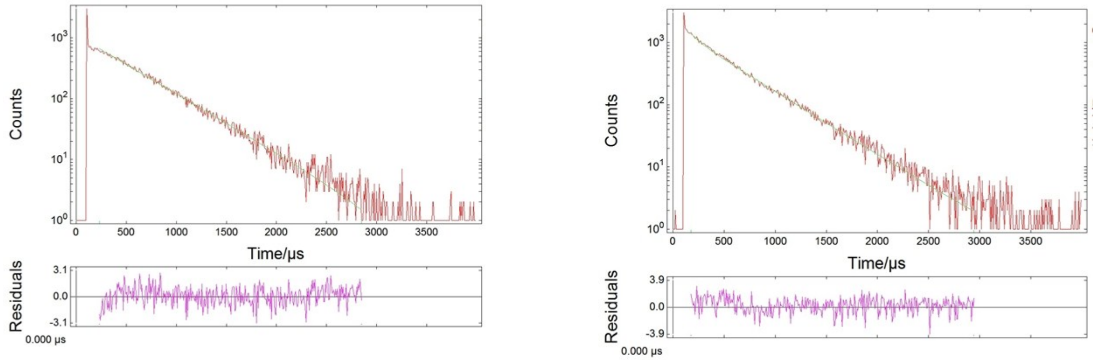

CP **11** CP **11**

Figure S4. Selected decay curves monitored at 618 nm (left side) and 547 nm (right side).

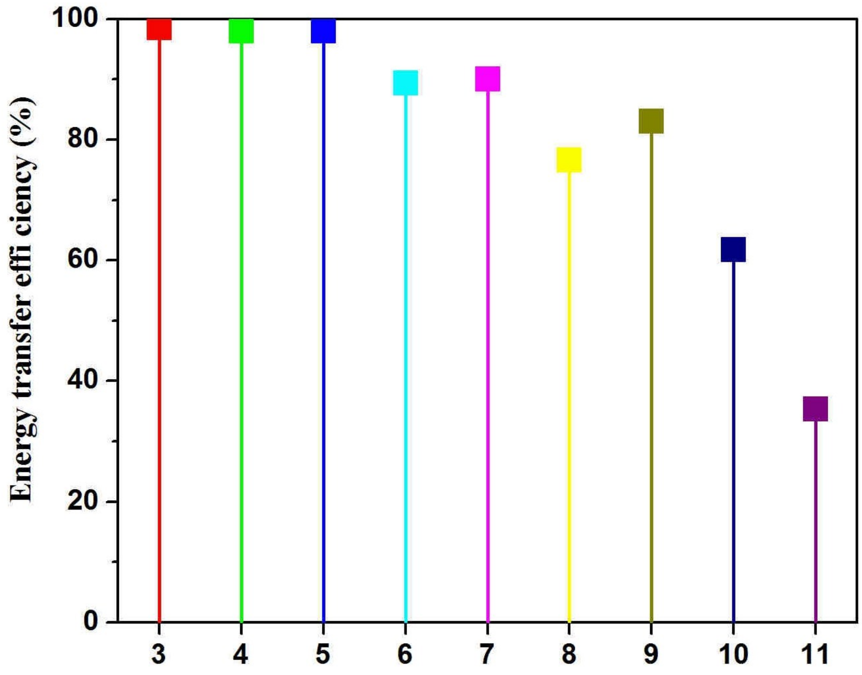

Figure S5. The energy transfer efficiency from Tb^{3+} to Eu^{3+} within CPs **3**–**11**.

2. Thermal and Water Stability

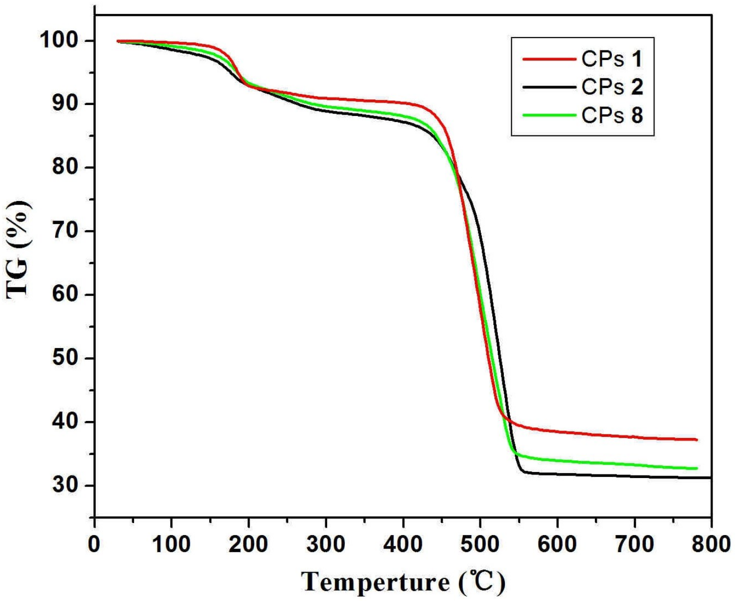

Figure S6. Thermogravimetric analyses (TGA) curve of CPs **1-2**, **8**.

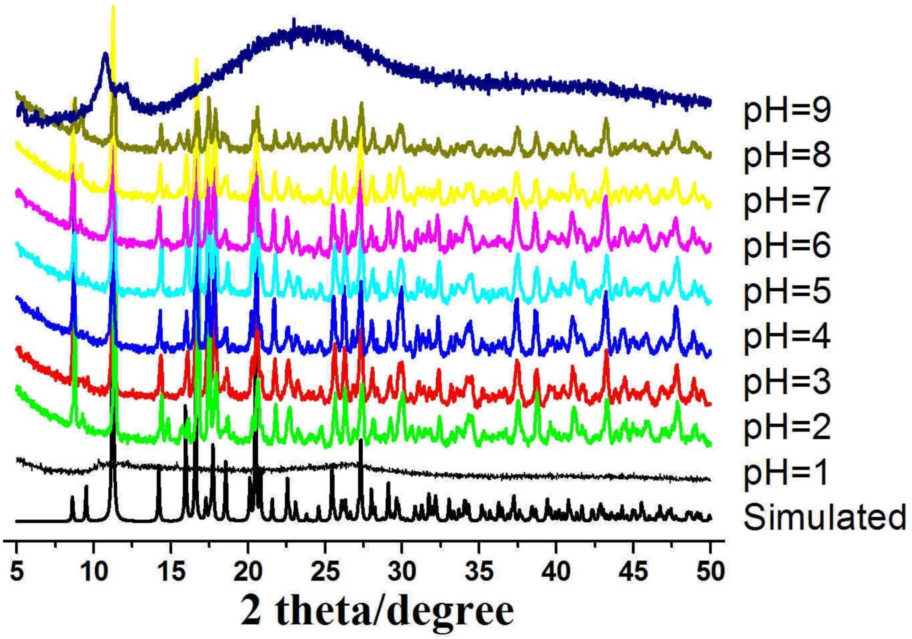

Figure S7. The PXRD patterns of **1** after exposure to aqueous solution with various pH values from 1.0 to 9.0.

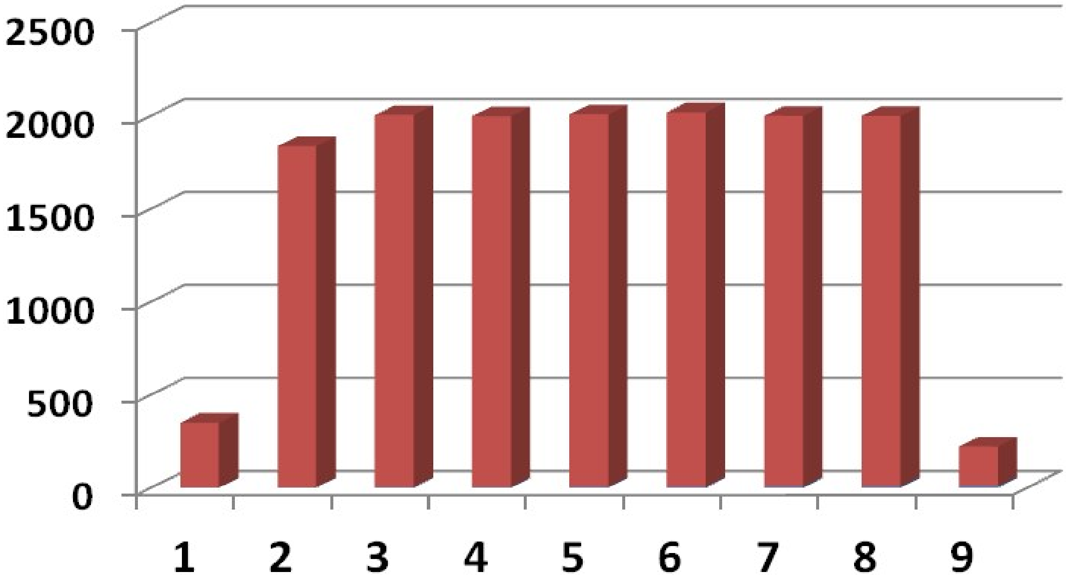

Figure S8. Comparison of the dominated emission peaks (618 nm) of **1** after exposure to various aqueous solutions with pH values from 1.0 to 9.0 (λ_{ex} = 321 nm).

3. Sensing of Metal Cations

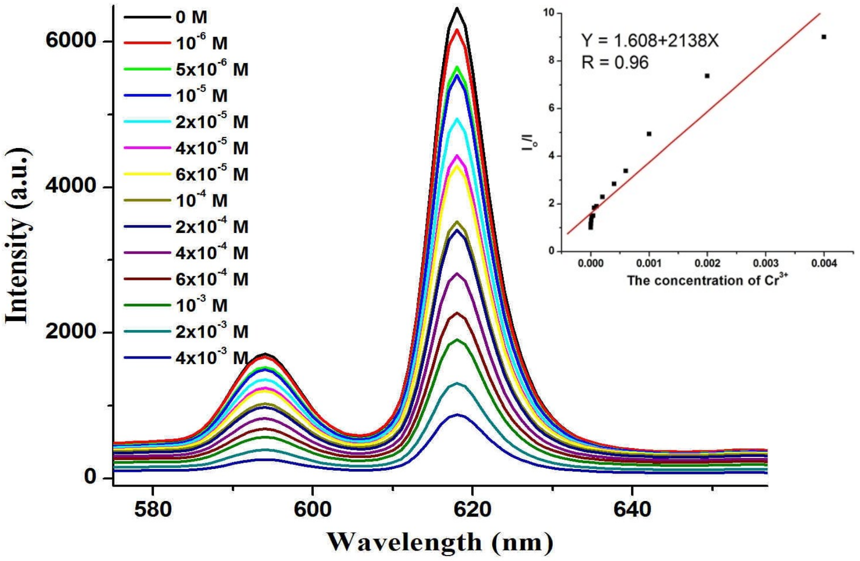

Figure S9. The luminescence intensity of CP **1** upon addition of different concentrations of $Cr(NO_3)_3$ aqueous solutions (λ_{ex} = 321 nm), (inset) the dose-response graph at 618 nm revealing the Stern−Volmer quenching constant K_{SV} was 0.0021 μM^{-1} for the luminescence quenching of **1** by Cr^{3+} based on the Stern-Volmer equation ($I_0/I = 1+K_{SV}[Q]$, I is the luminescence intensity at 6 nm with Fe^{3+} ions in solution while I_0 is in initial state. K_{SV} is the Stern-Volmer quenching constant, and [Q] is the concentration of quencher Cr^{3+}).

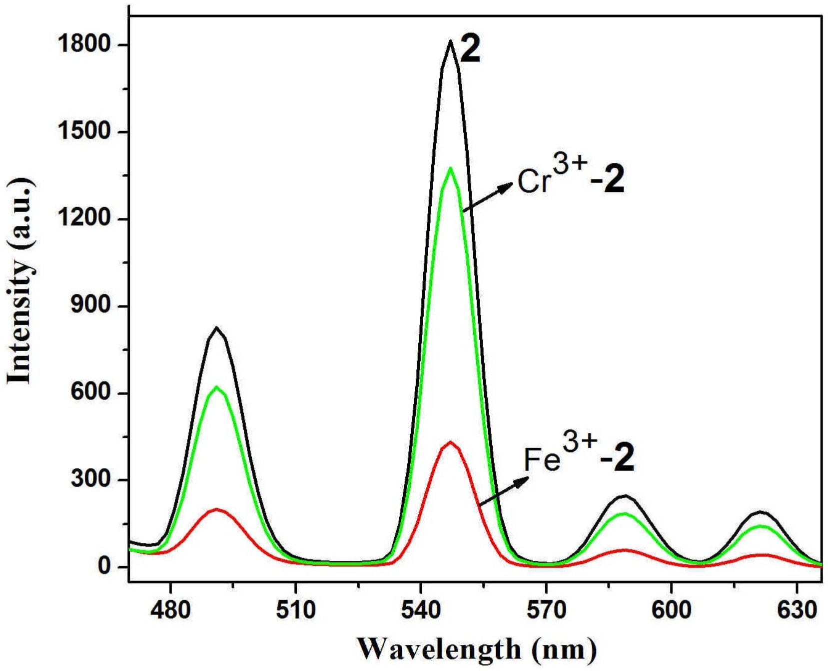

Figure S10. The luminescent spectra of **2** in the presence of Fe^{3+} and Cr^{3+} ions 10^{-3} M aqueous solutions (λ_{ex} = 331 nm).

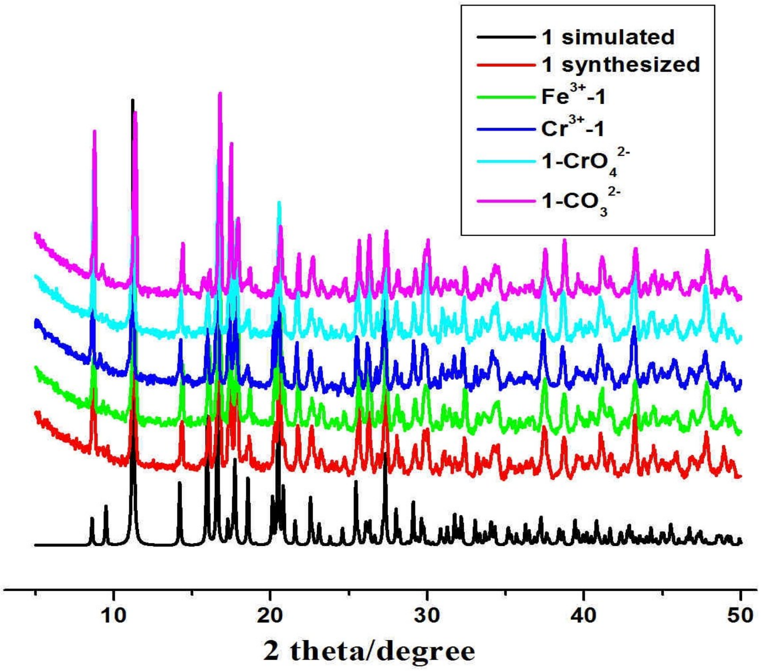

Figure S11. Powder XRD of simulated from the single-crystal data of **1** (black), as-synthesized **1** (red), **1** immersing in aqueous solution Fe^{3+}-**1** (green), Cr^{3+}-**1** (deep blue), **1**-CrO$_4^{2-}$ (light blue) and **1**-CO$_3^{2-}$ (purple).

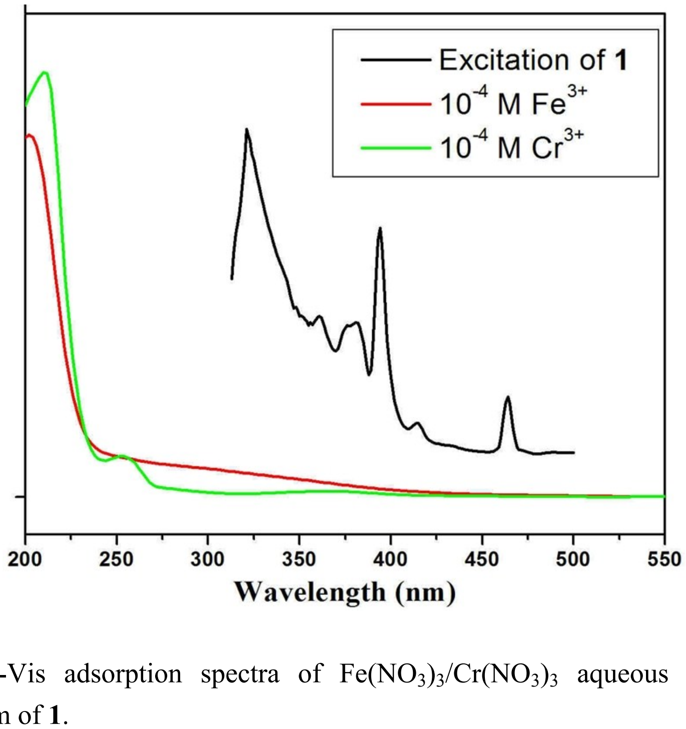

Figure S12. UV-Vis adsorption spectra of Fe(NO$_3$)$_3$/Cr(NO$_3$)$_3$ aqueous solutions and the excitation spectrum of **1**.

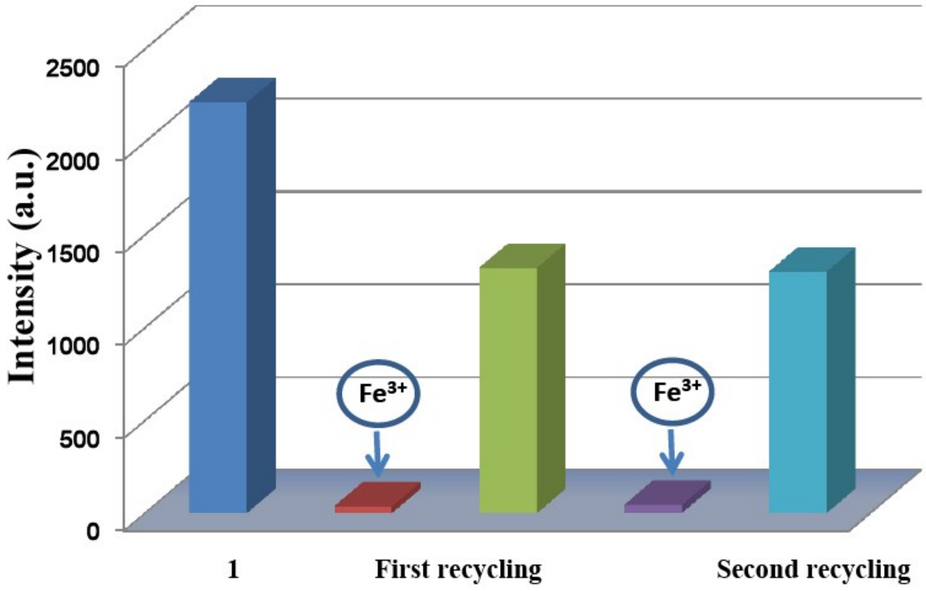

Figure S13. The luminescence intensity of **1** after two runs of recycling. The intensity is measured at 618 nm under the excitation wavelength of 321 nm.

4. Sensing of Anions

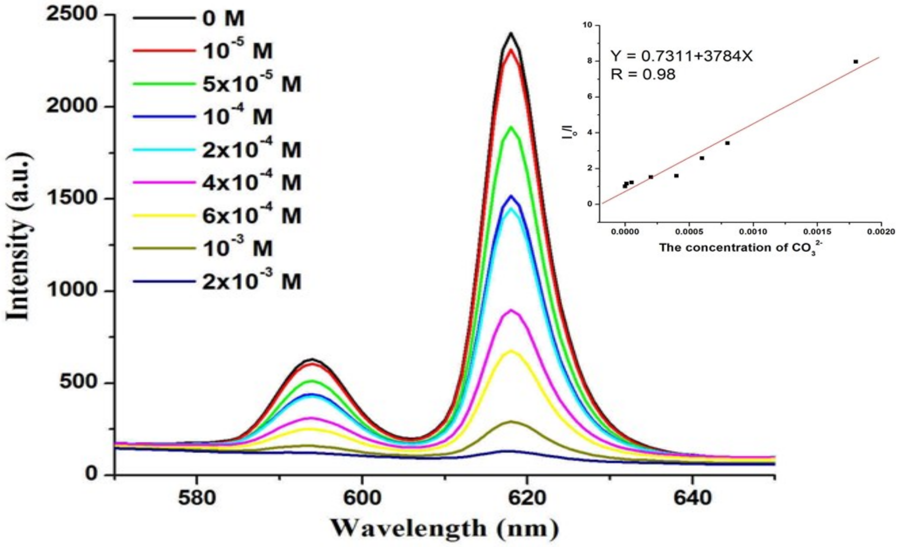

Figure S14. (a) The luminescence intensity of CP **1** upon addition of different concentrations of K_2CO_3 aqueous solutions, (inset) the dose-response graph at 618 nm revealing the Stern−Volmer quenching constant K_{SV} was 0.0231 μM^{-1}; (b) the luminescence intensity of **1** in different concentrations of K_2CO_3 aqueous solutions, (inset) the dose-response graph at 618 nm revealing the Stern−Volmer quenching constant K_{SV} was 0.0038 μM^{-1} (λ_{ex} = 321 nm).

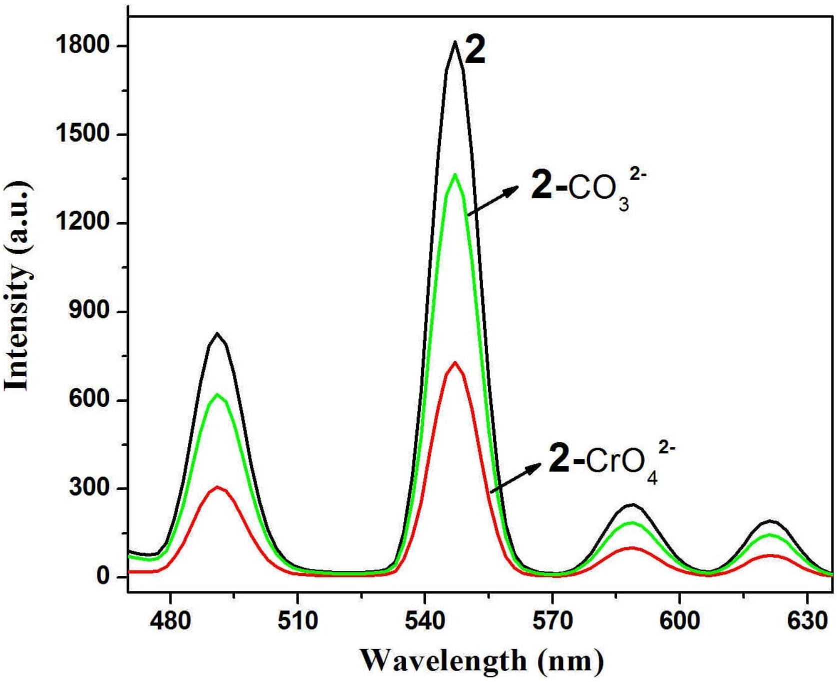

Figure S15. The luminescence intensity of **2**-X^{n-} in 10^{-3} M CrO_4^{2-}/CO_3^{2-} anions aqueous solutions (λ_{ex} = 331 nm).

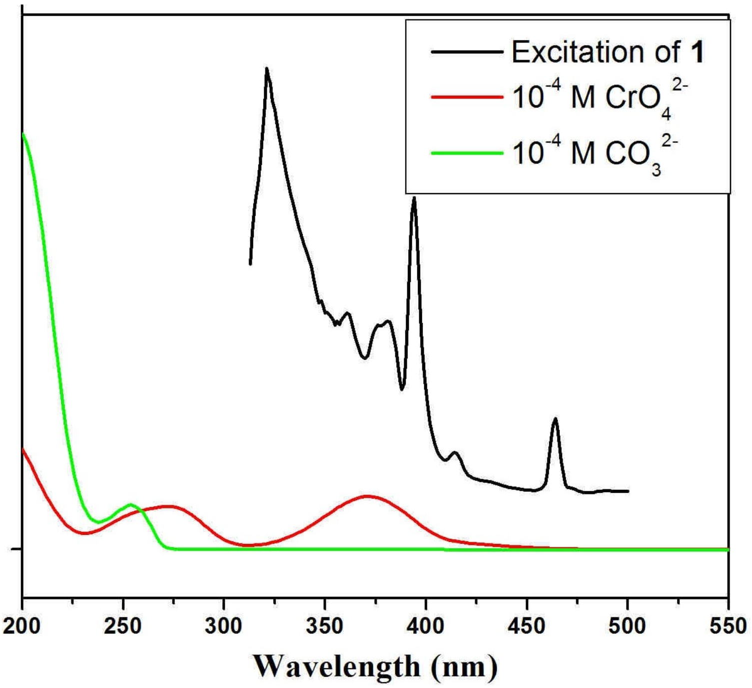

Figure S16. UV-Vis adsorption spectra of K_2CrO_4 / K_2CO_3 aqueous solutions and the excitation spectrum of **1**.

5. Sensing of Organic Solvent Molecules

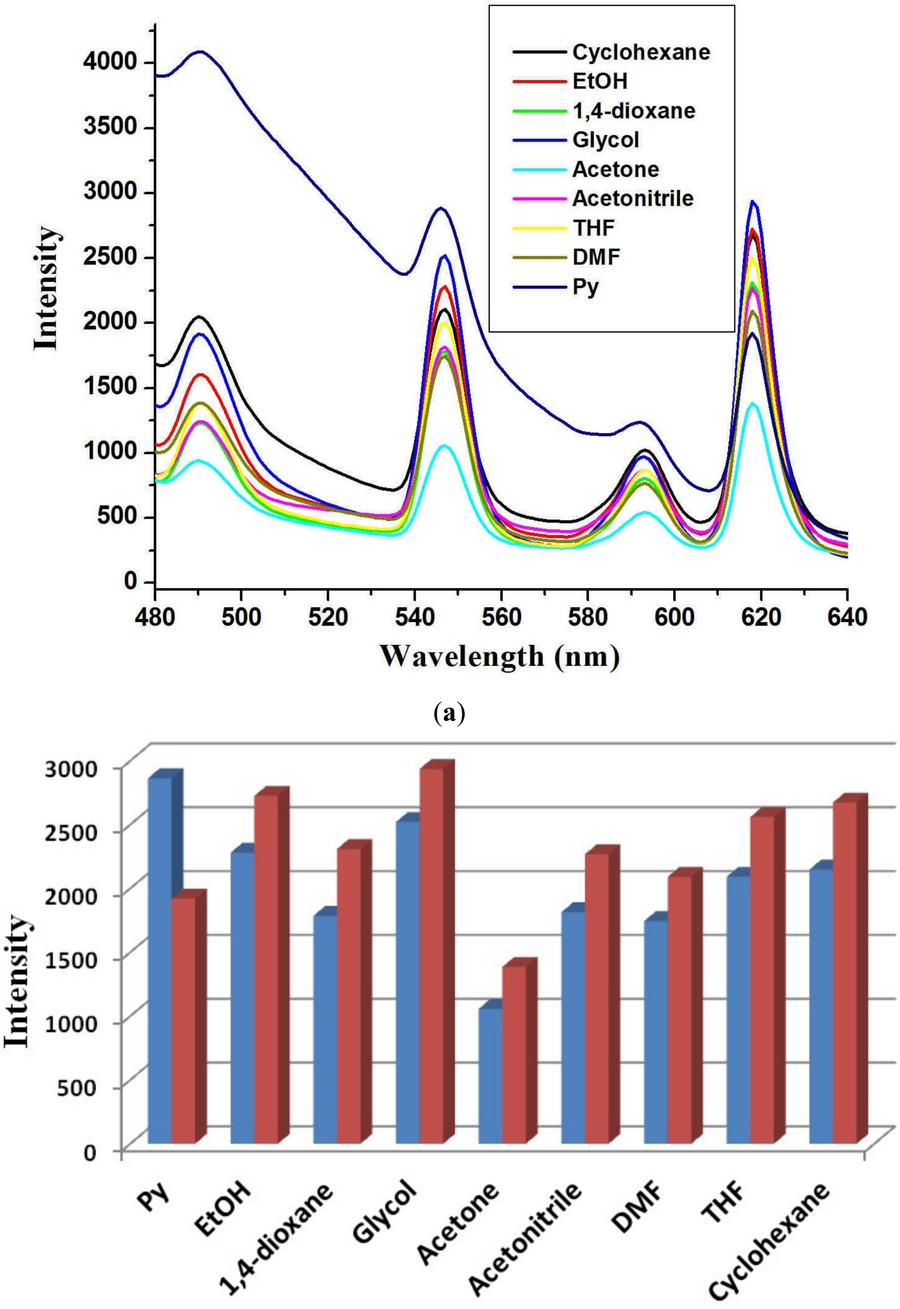

(a)

(b)

Figure S17. The luminescence emission spectra (a) and emission intensity of ${}^5D_4 \rightarrow {}^7F_5$ (Tb^{3+}, 547 nm, blue column) to ${}^5D_0 \rightarrow {}^7F_2$ (Eu^{3+}, 618 nm, red column) (b) in **8** after adsorption of pyridine (Py), EtOH, 1,4-dioxane, glycol, acetone, acetonitrile, DMF, tetrahydrofuran (THF), and cyclohexane excited at 331 nm at room temperature.

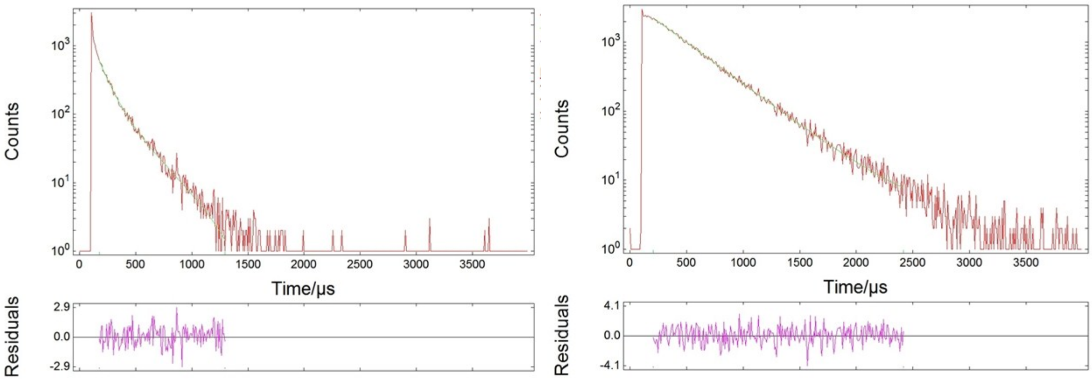

(a) (b)

Figure S18. Selected decay curves monitored at 547 nm (a) and 618 nm (b) for solid sample **8** after adsorption of pyridine.

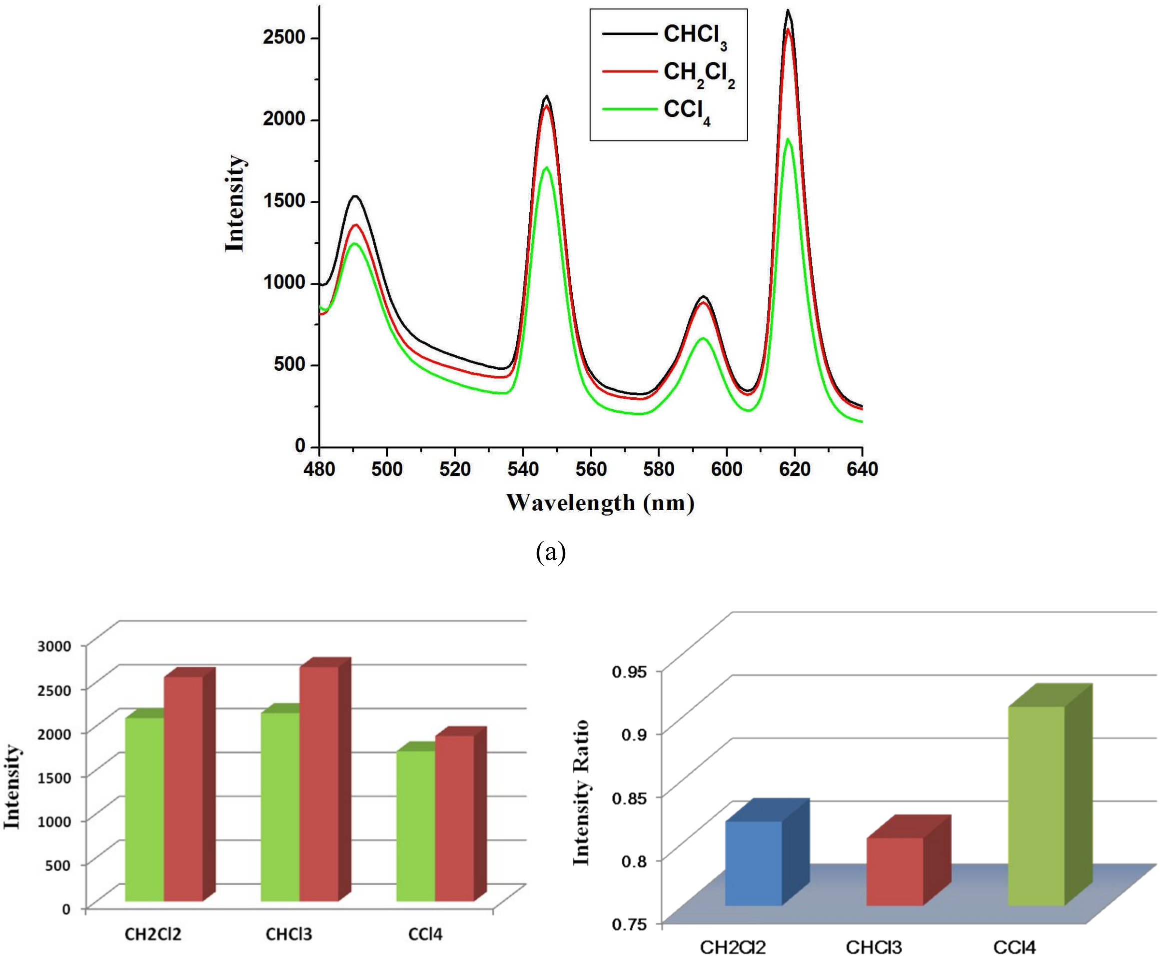

(a)

(b) (c)

Figure S19. The photoluminescence spectra (a), emission intensity of $^5D_4 \rightarrow {}^7F_5$ (Tb^{3+}, 547 nm, green column) and $^5D_0 \rightarrow {}^7F_2$ (Eu^{3+}, 618 nm, red column) (b) and emission intensity ratio of $^5D_4 \rightarrow {}^7F_5$ (Tb^{3+}, 547 nm) to $^5D_0 \rightarrow {}^7F_2$ (Eu^{3+}, 618 nm) (c) in suspension-state **8** after adsorption of dicloromethane (CH_2Cl_2), chloroform ($CHCl_3$) and tetrachloromethane (CCl_4) molecules, respectively, excited at 331 nm in the suspensions at room temperature.

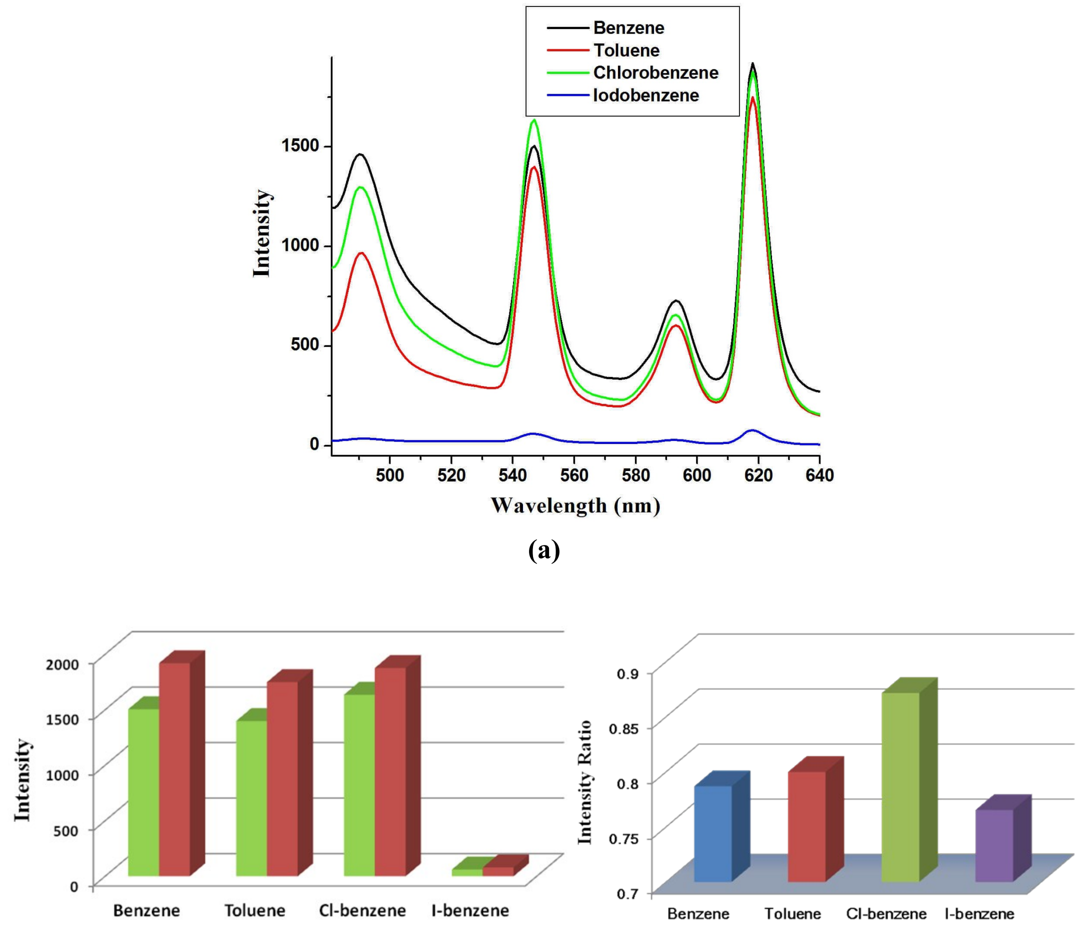

(a)

(b) (c)

Figure S20. The photoluminescence spectra (a), emission intensity of $^5D_4 \rightarrow {}^7F_5$ (Tb^{3+}, 547 nm, green column) and $^5D_0 \rightarrow {}^7F_2$ (Eu^{3+}, 618 nm, red column) (b) and emission intensity ratio of $^5D_4 \rightarrow {}^7F_5$ (Tb^{3+}, 547 nm) to $^5D_0 \rightarrow {}^7F_2$ (Eu^{3+}, 618 nm) (c) in suspension-state **8** after adsorption of benzene, toluene, chlorobenzene, and iodobenzene molecules, respectively, excited at 331 nm in the suspensions at room temperature.

6. Tables

Table S1. Crystal data and structure refinement for **1**.

Complex	**1**
Formula	$C_{18}H_{15}EuN_3O_{12}$
fw	617.29
T/K	293(2)
λ (Mo K), Å	0.71073
Cryst syst	Orthorhombic
Space group	*Fdd2*
a (Å)	11.538(2)
b (Å)	41.059(8)
c (Å)	17.067(3)
β(°)	90
V (Å^3)	8085(3)
Z	16
D_{calcd}.(g·cm^{-3})	2.028
Reflections collected /unique	13239 / 3675
abs coeff/mm^{-1}	3.179
F(000)	4848
θ (°)	2.19-25.49
GOF	1.082
R_1(I>2sigma(I))[a]	0.0398
wR_2(I>2sigma(I))[b]	0.0881

[a] $R_1 = \Sigma||F_o| - |F_c||/\Sigma|F_o|$ and [b] $wR_2 = \{\Sigma[w(F_o^2 - F_c^2)^2]/\Sigma[w(F_o^2)^2]\}^{1/2}$.

Table S2. The ICP analysis results of mixed Eu_xTb_{1-x}-CPs **3-11**.

Mixed Eu_xTb_{1-x}-CPs	Feed molar ratio （Tb:Eu）	Measured （Tb:Eu）
3	1:9	1.3:8.7
4	2:8	2.7:7.3
5	3:7	3.3:6.7
6	4:6	4.1:5.9
7	6:4	6.2:3.8
8	7:3	7:3
9	8:2	8:2
10	9:1	9.1:0.9
11	9.5:0.5	9.4:0.6

Table S3. The $^5D_4$ of Tb^{3+} and $^5D_0$ of Eu^{3+} lifetimes for CPs **1-11**. The decay curves are monitored at 547 nm and 618 nm and excited at 331 nm.

CPs	$^5D_4$ of Tb^{3+} /μs	$^5D_0$ of Eu^{3+} /μs
1	/	296.1
2	633.1	/
3	9.098	347
4	12.63	363.8
5	18.11	339.8
6	67.38	309.7
7	63.07	379.4
8	148.2	365
8[a]	182	360
9	106.6	408
10	242.4	392
11	409	450

8[a] : CP **8** solid after adsorption of pyridine.

Table S4. The ICP analysis results of Eu metal content of filtrate when CPs **1** immersed in a series of solutions with pH values ranging from 2 to 8.

pH	Measured（Eu : mg/L）
2	Non-detected
3	Non-detected
4	Non-detected
5	Non-detected
6	Non-detected
7	Non-detected
8	Non-detected